Vol. 678: 17–35, 2021
https://doi.org/10.3354/meps13879

MARINE ECOLOGY PROGRESS SERIES
Mar Ecol Prog Ser

Published November 11

Check for updates

OPEN ACCESS CC BY

Characterization of the biological, physical, and chemical properties of a toxic thin layer in a temperate marine system

Margaret A. McManus[1,*], Adam T. Greer[2], Amanda H. V. Timmerman[3], Jeff C. Sevadjian[4], C. Brock Woodson[5], Robert Cowen[6], Derek A. Fong[7], Stephen Monismith[7], Olivia M. Cheriton[8]

[1]Department of Oceanography, University of Hawai'i at Mānoa, Honolulu, HI 96822, USA
[2]University of Georgia, Skidaway Institute of Oceanography, Savannah, GA 31411, USA
[3]School of Marine Science and Policy, College of Earth, Ocean, and Environment, University of Delaware, Newark, DE 19716, USA
[4]Scripps Institution of Oceanography, University of California San Diego, La Jolla, CA 92037, USA
[5]School of ECAM Engineering, University of Georgia, Athens, GA 30601, USA
[6]Oregon State University, Hatfield Marine Science Center, Newport, OR 97365, USA
[7]Bob and Norma Street Environmental Fluid Mechanics Laboratory, Stanford University, Stanford, CA 94305, USA
[8]US Geological Survey, Pacific Coastal and Marine Science Center, Santa Cruz, CA 95060, USA

ABSTRACT: The distribution of plankton in the ocean is patchy across a wide range of spatial and temporal scales. One type of oceanographic feature that exemplifies this patchiness is a 'thin layer'. Thin layers are subsurface aggregations of plankton that range in vertical thickness from centimeters to a few meters, which may extend horizontally for kilometers and persist for days. We undertook a field campaign to characterize the biological, physical, and chemical properties of thin layers in Monterey Bay, California (USA), an area where these features can be persistent. The particle aggregates (marine snow) sampled in the study had several quantifiable properties indicating how the layer was formed and how its structure was maintained. Particles were more elongated above the layer, and then changed orientation angle and increased in size within the layer, suggesting passive accumulation of particles along a physical gradient. The shift in particle aggregate orientation angle near the pycnocline suggests that shear may also have played a role in generating the thin layer. *Pseudo-nitzschia* spp. were the most abundant phytoplankton within the thin layer. Further, both dissolved and particulate domoic acid were highest within the thin layer. We suggest that phosphate stress is responsible for the formation of *Pseudo-nitzschia* spp. aggregates. This stress together with increased nitrogen in the layer may lead to increased bloom toxicity in the subsurface blooms of *Pseudo-nitzschia* spp. Several zooplankton groups were observed to aggregate above and below the layer. With the knowledge that harmful algal bloom events can occur in subsurface thin layers, modified sampling methods to monitor for these hidden incubators could greatly improve the efficacy of early-warning systems designed to detect harmful algal blooms in coastal waters.

KEY WORDS: Thin layer · Harmful algal bloom · HAB · Monterey Bay · Phytoplankton · Zooplankton

1. INTRODUCTION

The spatial distribution of plankton in the ocean is patchy in both space and time (Lasker 1975, Bennett & Denman 1985, Bjørnsen & Nielsen 1991, Donaghay et al. 1992). While aggregations of plankton are readily observed at the surface, very dense, spatially extensive aggregations of plankton can also occur subsurface, within vertically narrow depth ranges, making them very difficult to detect by traditional

*Corresponding author: mamc@hawaii.edu

© The authors 2021. Open Access under Creative Commons by Attribution Licence. Use, distribution and reproduction are unrestricted. Authors and original publication must be credited.

Publisher: Inter-Research · www.int-res.com

observing methods such as remote sensing, bottle samples, or discrete-depth instruments. These features, called 'thin layers', can be highly productive and can contain multiple strata of organisms and organic material, including harmful algal bloom (HAB) species. Thin layers range in thickness from a few centimeters to a few meters, may extend horizontally for kilometers, and may persist for days (Dekshenieks et al. 2001). Understanding the biological, physical, and chemical mechanisms driving this patchiness will allow us to predict patterns of heterogeneity in coastal areas around the globe. This is critical knowledge as we move into an unprecedented period in history, as our oceans' biological populations, chemistry, and physical structures change with rising average global temperatures and other sources of anthropogenic influence.

Since their discovery in the 1960s (Strickland 1968), thin layers have been detected in both coastal and open ocean waters worldwide. The bulk of these observations were made from the late 1990s to 2014, driven by a rapid advancement in sampling methods and technologies involving optical sensing (Cowles et al. 1998, Dekshenieks et al. 2001, McManus et al. 2003), acoustic sensing (Holliday et al. 2003, McManus et al. 2005, Cheriton et al. 2007, Sevadjian et al. 2010, Benoit-Bird & McManus 2012), underwater imaging (Alldredge et al. 2002, Greer et al. 2013), towed vehicles (Cheriton et al. 2009, 2010), autonomous underwater vehicles (Ryan et al. 2008, 2010, Hodges & Fratantoni 2009), and airplane-based light detection and ranging (Churnside & Donaghay 2009).

Additional interest in thin layers was stimulated by the discovery that the onset of many HAB events goes undetected because the HAB is initially concentrated in discrete thin subsurface layers in the water column; these layers are easily missed by conventional sampling and monitoring methods (McManus et al. 2008, Berdalet et al. 2014, Raine et al. 2014, Ryan et al. 2014, Sevadjian et al. 2014, Timmerman et al. 2014).

Monterey Bay, California (USA), has been a focal point for many investigations of thin layers. Work in this system provided much of the observational foundation for our current understanding of the mechanisms generating thin layers. The bay is highly productive and economically important in terms of both fishing and tourism, and it has been identified as a key HAB monitoring site and 'hot spot' for the West Coast (Scholin et al. 2000, Trainer et al. 2000). HABs are often observed in thin layers in this region (McManus et al. 2008, Ryan et al. 2010, 2014, Greer et al. 2013, Timmerman et al. 2014).

In this study, several instruments were deployed in Monterey Bay in a comprehensive and complementary configuration to elucidate and quantify the biological, physical, and chemical properties of thin layers. Our results contribute a broad understanding of the fundamental processes structuring the plankton communities on the Monterey Bay shelf, and add to our understanding of the mechanisms of thin layer formation and their subsequent ecological impacts.

2. MATERIALS AND METHODS

2.1. Study area

Monterey Bay is a semi-enclosed bay located between 36.5 and 37° N on the central coast of California. An array of instruments was located in a study area in the northeast region of Monterey Bay where a well-characterized upwelling shadow, a warm shallow lens of water trapped by topography, has been observed (Graham & Largier 1997) (Fig. 1).

2.2. Wind and tide data

Wind velocity and tidal stage data were obtained from nearby stations and provide an important physical context for the measurements taken in this oceanographic study. Regional wind data were obtained from the National Oceanic and Atmospheric Administration National Data Buoy Center (NOAA/NDBC) buoy number 46042 (36.789° N, 122.404° W) (www.ndbc.noaa.gov) located 51 km to the west-southwest of the study area. Local wind data were obtained from a weather station at Long Marine Laboratory 13 km west-northwest of the study area. Six-minute tidal height data were obtained from the NOAA Monterey tide gauge (http://tidesandcurrents.noaa.gov).

2.3. Water column profiling

2.3.1. SeaHorse

A SeaHorse autonomous vertical profiler (ODIM Brooke Ocean) was deployed at the 20 m isobath, near the center of the array from 27 June to 9 July 2010 (Fig. 1). The SeaHorse uses wave energy to continuously profile the water column. The payload is slightly positively buoyant, and sensor data are collected during ascending profiles. Upon reaching the surface, a wave-driven, wire-gripping mechanism

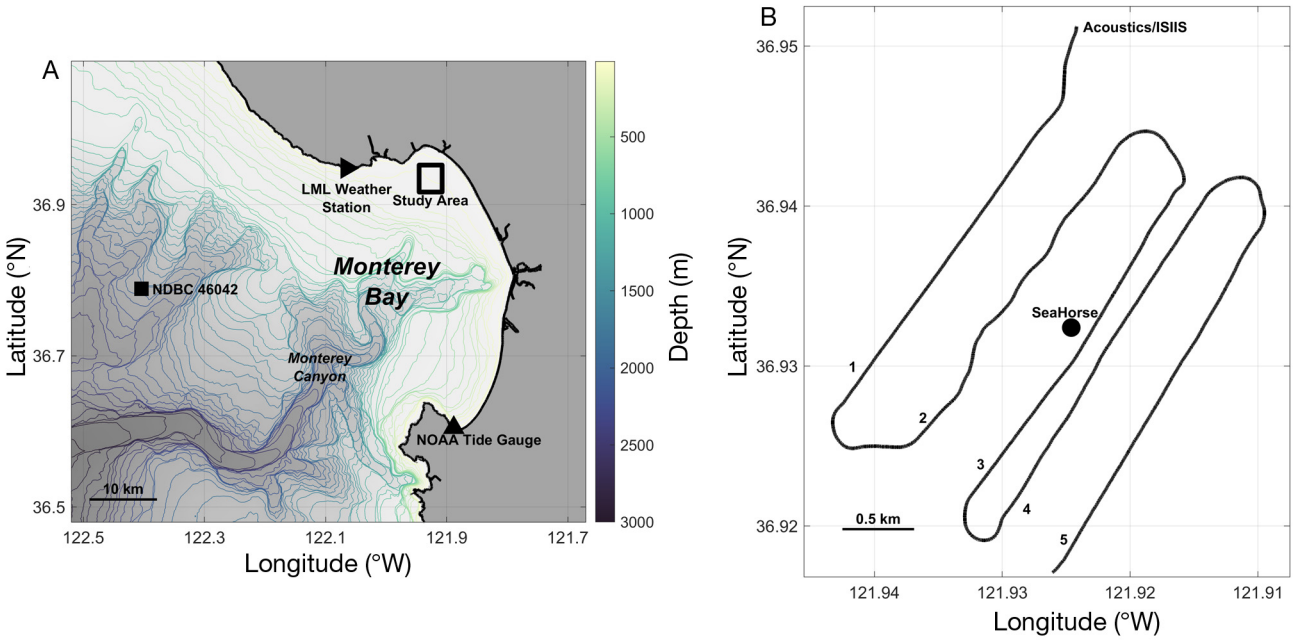

Fig. 1. (A) Study area in Monterey Bay, California (USA), showing the locations of the Long Marine Laboratory (LML) weather station, National Oceanic and Atmospheric Administration National Data Buoy Center (NOAA NDBC) wave buoy 46042, and NOAA tide gauge. (B) Enlargement of study area with acoustic/*in situ* ichthyoplankton imaging system (ISIIS) boat tracks and SeaHorse profiler mooring (black circle). Numbers 1–5 correspond to acoustic/ISIIS transect numbers in Figs. 5 & 7

returns the payload to depth. The SeaHorse collected profiles from 5 m above the bottom to 1 m depth every 30 min. The sensor payload included a Sea-Bird Electronics (SBE) model 19+ CTD, SBE-43 oxygen sensor, and WETLabs WetSTAR chlorophyll fluorometer, each sampling at 4 Hz, resulting in a vertical resolution of ~8 cm. Each sensor was factory-calibrated prior to the study. During the latter portion of the study, the wire-gripping mechanism began to foul and occasionally the package did not return to depth after completing a profile.

2.3.2. High-resolution profiler

A high-resolution profiling package was utilized from 10:29 to 14:02 h on 5 July aboard a 10 m vessel (RV 'Paragon', 36.9324° N, 121.9246° W) at a 20 m horizontal distance from the SeaHorse moored profiler (Fig. 1). The high-resolution profiler profiled the water column (1 to ~21 m) with high temporal (~5 min) and spatial (<1 cm) resolution. The high-resolution profiler was equipped with an SBE-25 CTD (8 Hz), SBE-43 oxygen sensor (8 Hz), ISUS nitrate sensor (8 Hz), and WET Labs ac-9 spectral absorption and attenuation meter (6 Hz).

The ac-9 absorption at 676 nm (ap676) and 650 nm (ap650) were used to estimate chlorophyll *a* (chl *a*) concentration based on Mobley et al. (2002) using Eq. (1):

$$\text{chl}\,a = \frac{\text{ap676} - \text{ap650}}{0.014} \quad (1)$$

The high-resolution profiler was unaffected by boat movement because it was designed to be on a slack tether and slightly negatively buoyant. The high-resolution profiler was released to profile with an average descent rate of 13.2 cm s^{-1}, achieving a vertical resolution of <1 cm.

After Dekshenieks et al. (2001), peaks in the chl *a* profiles had to meet several criteria in order to be considered thin layers. First, the chl *a* peak was required to be at least 3 times greater than background values. Second, the vertical thickness of the peak (measured where the optical peak was a half maximum intensity) had to be no thicker than 5 m. Finally, the optical signal had to be present in 2 or more subsequent profiles with the high-resolution profiler. These are conservative criteria, which are designed to eliminate ephemeral features or 'patches' not associated with a coherent layer (Dekshenieks et al. 2001).

2.4. Bottle samples

A 5 l Aquatic Research Instruments discrete point water-sampling bottle was attached to the high-resolution profiler to collect water samples. Real-time data of depth and fluorescence from the high-resolution profiler allowed accurate water sampling from above, within, and below thin layers of fluorescence. Water samples were collected at 13:08, 13:22, and 13:36 h at depths of 7.4, 15.2, and 4 m, respectively. Water samples were gently mixed in a carboy before subsampling. Brief descriptions are provided below. For more detailed information on the bottle samples, see Timmerman et al. (2014). All samples were analyzed or processed within 5 h after returning from the field.

Unfixed triplicate phytoplankton samples were identified and enumerated to genus level using a Zeiss A1 Axioscope microscope (40× magnification) and a PhycoTech 0.066 ml phytoplankton counting cell.

For bacteria enumeration, samples were preserved with paraformaldehyde (0.5% final concentration), then stored at −80°C until batch analyses. Thawed samples were stained for 1 h with Hoechst 33342 (1 µg ml^{-1} final concentration), then analyzed on a Beckman Coulter EPICS Altra flow cytometer (Selph et al. 2005).

Volumes of 750 ml to 1 l were filtered through acid-cleaned 47 mm diameter, 0.2 µm GHP filters. The filters were stored frozen for later determinations of cell-associated alkaline phosphatase activity (APA), a proxy for phosphorus stress, following Dyhrman & Ruttenberg (2006). The filtrate was frozen in acid-cleaned bottles until analyzed for dissolved nutrients (NO_3^-, NO_2^-, NH_4^+, PO_4^{3-}, $Si(OH)_4$), total dissolved nitrogen (TDN), and total dissolved phosphorus (TDP) at the University of Washington Water Center (Marine Chemistry Laboratory).

Three aliquots were filtered for dissolved and particulate domoic acid determinations. The filtrate from GF/F filters was collected and frozen in bottles (acid washed) for dissolved domoic acid (dDA). GHP filters (47 mm diameter, 0.2 µm) were used to determine particulate domoic acid (pDA). Samples were analyzed following Wang et al. (2007) on an Agilent 6130 LC/MS using Selective Ion Monitoring.

Pre-weighed 47 mm diameter, 0.2 µm GHP filters were used to collect material for determination of total suspended solids (TSS). TSS filters were dried until the post-weights were stable (<0.16% difference), then the pre-weight was subtracted and divided by the volume of water filtered (750 ml).

2.5. Towed and shipboard systems

2.5.1. *In situ* ichthyoplankton imaging system (ISIIS)

The ISIIS is a towed shadowgraph imaging system that synoptically measures oceanographic properties, including salinity, temperature, depth (SBE49, SeaBird Electronics), and chl *a* fluorescence (ECO FL (RT), WETLabs). The camera pods contain a line scan camera (Dalsa) with 68 µm pixel resolution on one side, and an LED light source on the other side that projects collimated light across an imaged water parcel (13 cm high field of view) into the camera. Due to the high concentrations of plankton and particles in this region, the depth of field was conservatively estimated to be ~35 cm. This optical technique allowed particles and plankton between ~500 µm and 13 cm to be imaged and identified. Along with the camera system, the ISIIS was equipped with motor actuated fins for depth control, a Doppler velocity log (600 micro, Navquest), and environmental sensors all measuring at 2 Hz. All sensors sampled water ~0.5 m above the imaging volume, and a correction was applied to correct for this offset. The system was deployed off the stern of a 15.85 m coastal vessel, the RV 'Shana Rae', towed at a constant speed of 2.5 m s^{-1} through the water, with ~4–5 undulations, from ~1 m under the surface to ~5 m above the bottom, reaching a maximum depth of ~18 m. A total of 5 transects centered over the 20 m isobaths were surveyed during afternoon hours on 5 July 2010 between 12:32 and 14:14 h (Fig. 1). Due to the optical technique utilized by the ISIIS, ambient light has no effect on image quality (Cowen & Guigand 2008).

The images obtained from the ISIIS were processed using a series of steps. First, the images were flat-fielded to remove background artifacts from the line scan camera (i.e. thin vertical lines) and to even out the background gray level. Images were then segmented using the image analysis software ImageJ (Schneider et al. 2012), which applied a threshold to the image (i.e. converting to black and white) for a gray level of 170 (on a scale from 0 to 255, 8-bit grayscale images) and extracted all particles ≥2000 pixels in cross-sectional area (~3.3 mm equivalent spherical diameter; ESD) as regions of interest (ROIs), along with several particle statistics, including particle cross sectional area,

perimeter, major/minor axes of a fitted ellipse to each particle (used to calculate aspect ratio), and angle of the major axis. A random subset of 2000 ROIs was classified manually to determine the percentage of segments that were marine snow particles. In addition, several particle characteristics were recorded as already described. These particle statistics (measured for each particle) were merged with the environmental data using the image/environmental data timestamps and were then placed into 1 m bins. Using the known camera field of view, depth of field, and speed of the ship, volume sampled for each vertical bin was calculated, and the number of particles could then be converted to concentrations per sample bin. This analysis and plotting was performed in R (v.3.2.2) using the packages 'plyr' and 'ggplot2' (Wickham 2011, 2016)

To compare the particle statistics, particles from waters well above (2–3 m), within (6.5–7.5 m), and well below (14–15 m) the thin layer were extracted for further analysis. Mean particle area (in pixels) and concentration were calculated for the 3 depth groups. For other particle statistics, including perimeter to area ratio, aspect ratio, and angle of orientation, the data were log transformed to conform to assumptions of parametric statistics, and an ANOVA was run for the different measurements. Tukey's post hoc HSD test was used to indicate statistically significant differences among the depth zones.

2.5.2. Acoustics

Acoustic surveys were conducted from the RV 'Shana Rae' on 5 July 2010 between 12:32 and 14:14 h using a Simrad EK60 split-beam echosounder with a 200 kHz transducer mounted to a bracket attached to the vessel gunwale. A 200 kHz acoustic signal is expected to scatter off of objects in the size range of small zooplankton, including invertebrate larvae (300 µm and larger; Clay & Medwin 1977). Acoustic profiles of the water column were taken at 2 Hz with the vessel moving at 2.5 m s^{-1}, resulting in a horizontal resolution of 1.25 m. The 200 kHz transducer had a 20.7° beam angle and used a 64 µs pulse, resulting in 1.2 cm vertical bins. Raw, binary EK60 backscatter data were read into Matlab and converted from echo return power in units of W, to volume backscattering strength (S_V) in units of dB m^{-1}, using a Matlab toolbox (R. Towler unpubl. data), assuming a sound absorption coefficient of 0.057 dB m^{-1}. The EK60 echosounder was factory-calibrated prior to the study.

2.6. Co-occurrence of sensors and platforms on 5 July

Continuous measurements of wind velocity and tidal height were available for the day of 5 July. Near-continuous profiles from the SeaHorse were available from ~04:30 to 09:30 and 21:30 to 23:30 h, and from the high-resolution profiler from 10:29 to 14:02 h. Bottle samples were collected within this time frame at 13:08, 13:22, and 13:36 h. Surveys with the ISIIS and acoustics took place between 12:32 and 14:14 h (Table 1).

3. RESULTS

3.1. Winds and tides

From 29 June to 4 July, the regional winds were consistently from the northwest, averaging 7.0 m s^{-1}; these are typical upwelling winds. On 4 July, the regional winds shifted, and from 4 to 8 July, they were consistently from the south, averaging 3.7 m s^{-1}. From 29 June to 4 July, the local winds had a typical diurnal (sea breeze) signal, with onshore winds increasing from late morning to early afternoon, and decreasing into the evening. Then, from 4 to 9 July, the local wind speeds decreased to well below 3 m s^{-1}, likely due to the decrease in amplitude of air temperature fluctuations during the same time frame. The third-quarter moon (half-moon) was on 4 July, thus the period of sampling occurred over neap tide when the tidal range and tidal current velocities are relatively lower. The average magnitude over the entire record was 0.074 m s^{-1}, while average current magnitude on 5 July was 0.036 m s^{-1}. During the time of the study, offshore significant wave height was low, ~2 m, and from the south (180°) (Fig. 2). Due to the location of the study site, situated in the north-

Table 1. Time of day on 5 July 2010 and data availability of winds, tides, SeaHorse autonomous vertical profiler, high-resolution profiler, bottle sampling, *in situ* ichthyoplankton imaging system (ISIIS), and acoustics. All times are in local Pacific daylight savings time

	Time of day (h)
Wind	00:00–23:59
Tide	00:00–23:59
SeaHorse	04:30–09:30, 21:30–23:30
High resolution	10:29–14:02
Bottle samples	13:08, 13:22, 13:36
ISIIS	12:32–14:14
Acoustics	12:32–14:14

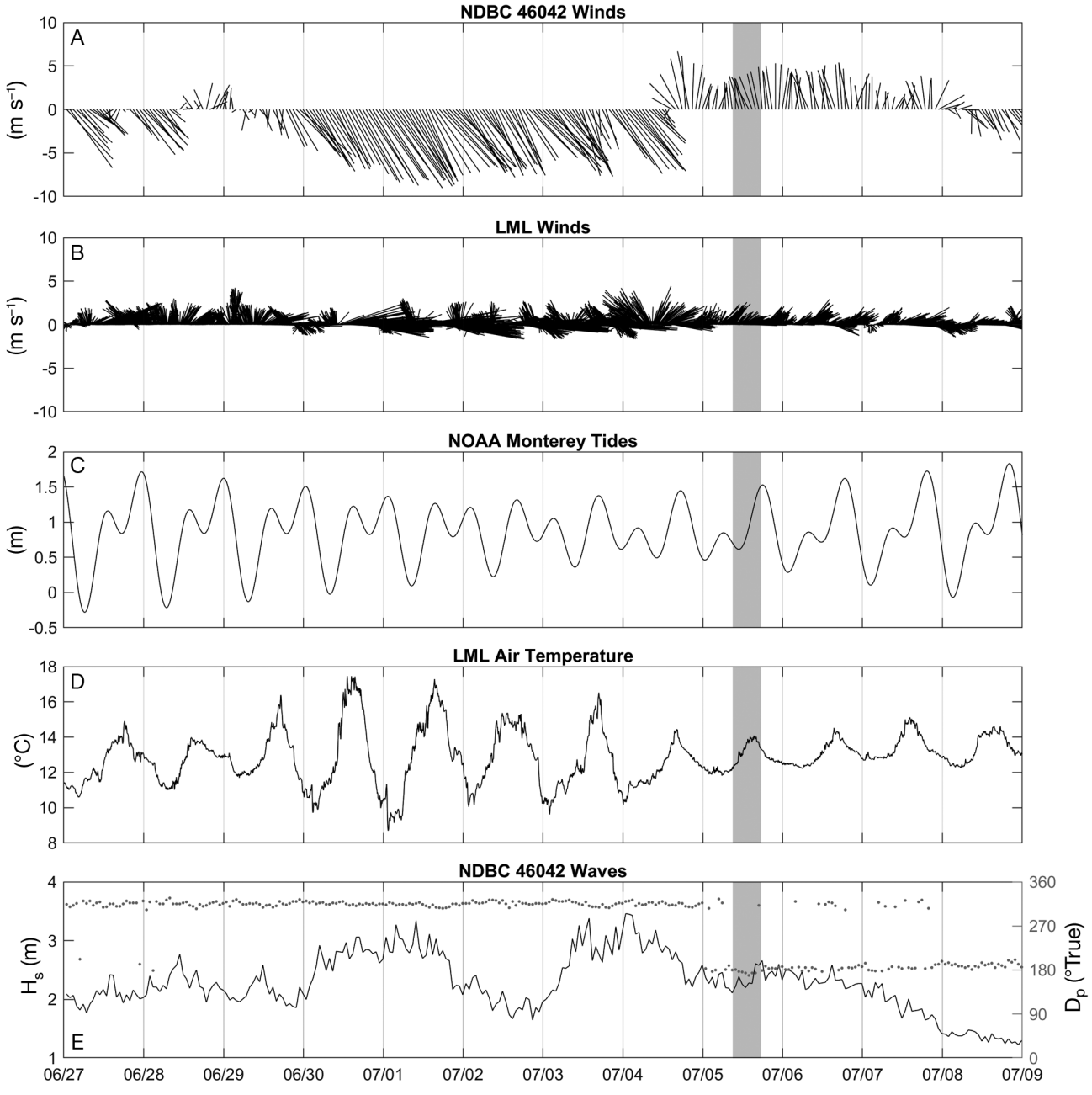

Fig. 2. (A) Regional winds (m s^{-1}) measured at NDBC buoy 46042, from 27 June to 9 July 2010. Wind direction is represented by the angle of the vector, and wind magnitude is represented by the length of the vector. (B) Local winds (m s^{-1}) measured at Long Marine Laboratory (LML) from 27 June to 9 July 2010. (C) Predicted tides from the NOAA Monterey tide station. Sea level height is in m. (D) Air temperature (°C) at LML. (E) Significant wave height (H_s, m) and peak wave direction (D_p, °) from NDBC Buoy 46042. Time is local time (PDST). Shaded bar shows the measurement time span on 5 July

eastern corner of Monterey Bay, the southern swell and offshore winds did not have a large influence on the study region.

Notes from the small boat log indicated that conditions at 09:54 h were quiescent, calm, and foggy with light swell. By 11:24 h, the wind increased only slightly. By 13:22 h, there were intermittent, but mildly increased, swells, and winds remained light.

3.2. Water column profiling

3.2.1. SeaHorse profiler

A total of 467 profiles of temperature, salinity, fluorescence, and dissolved oxygen were collected with the SeaHorse profiler between 27 June and 9 July (Fig. 3); however, only a few profiles were collected

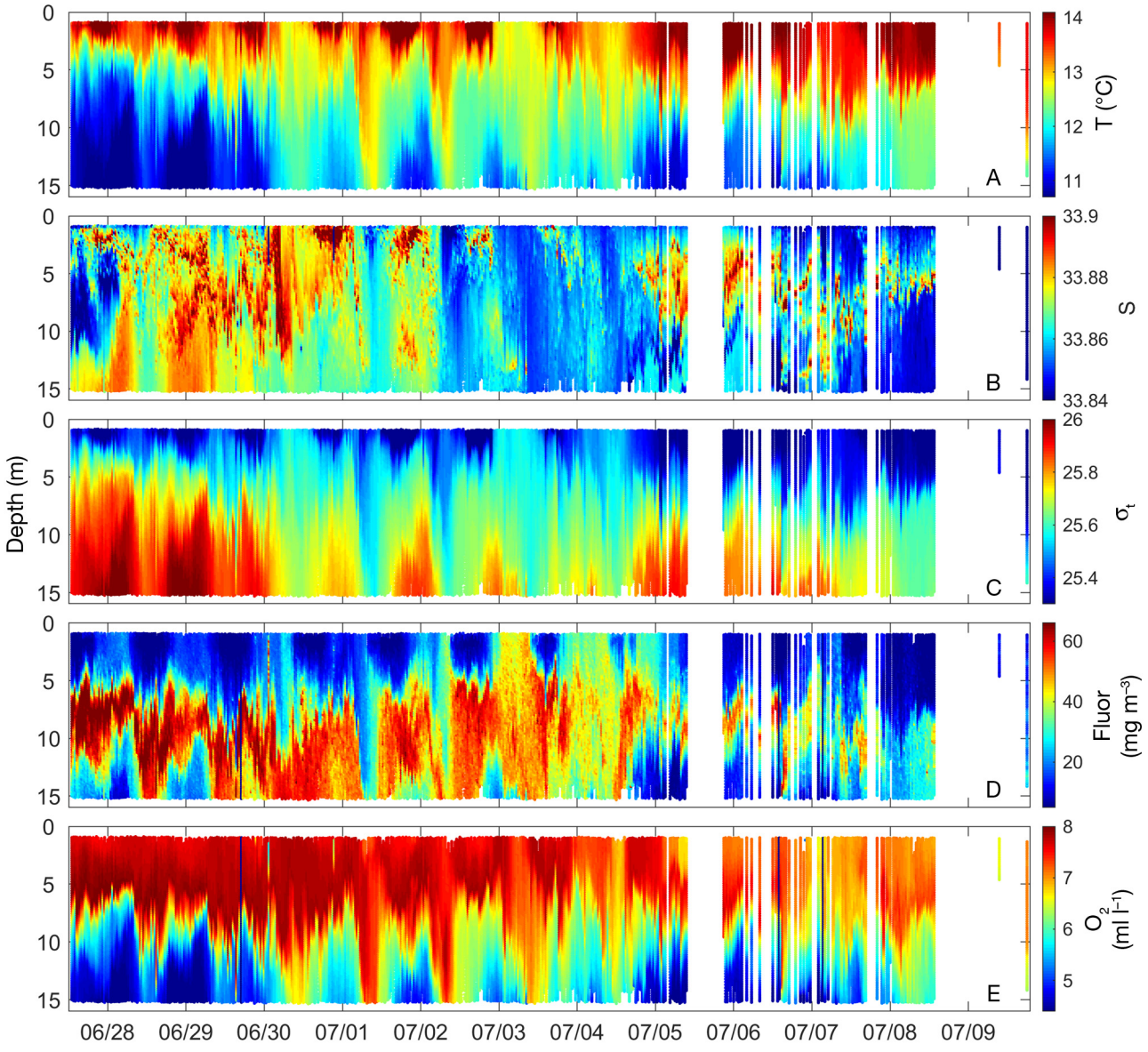

Fig. 3. Measurements from the SeaHorse profiler: (A) temperature (°C), (B) salinity, (C) density (σ_t), (D) fluorescence (mg m^{-3}) (the WETLabs Inc. factory calibration was to convert from volts to mg m^{-3}), (E) oxygen (ml l^{-1})

on 5 July due to fouling of the wire-gripping mechanism. Between 29 June and 4 July, there were periods where the water column was periodically mixed due to the local winds, which had a typical diurnal signal. From 4 to 7 July, the water column was stably stratified due to the decrease in local wind velocities to below 3 m s^{-1} coupled with neap tide (e.g. lower current velocities) and low wave energy. These conditions were optimal for the formation of the intense thin layer at the base of the pycnocline sampled on 5 July.

3.2.2. High-resolution profiler

A total of 37 profiles of temperature, salinity, absorption, dissolved oxygen, and dissolved inorganic nitrate were manually collected with the high-resolution profiler between 10:29 and 14:02 h (3 h, 33 min) on 5 July (Fig. 4), with an average of 5 min between each profile. Of these, 4 profiles did not cover the full depth range and were excluded from analyses. The water column was strongly stratified. The pycnocline (27.5 sigma-t)

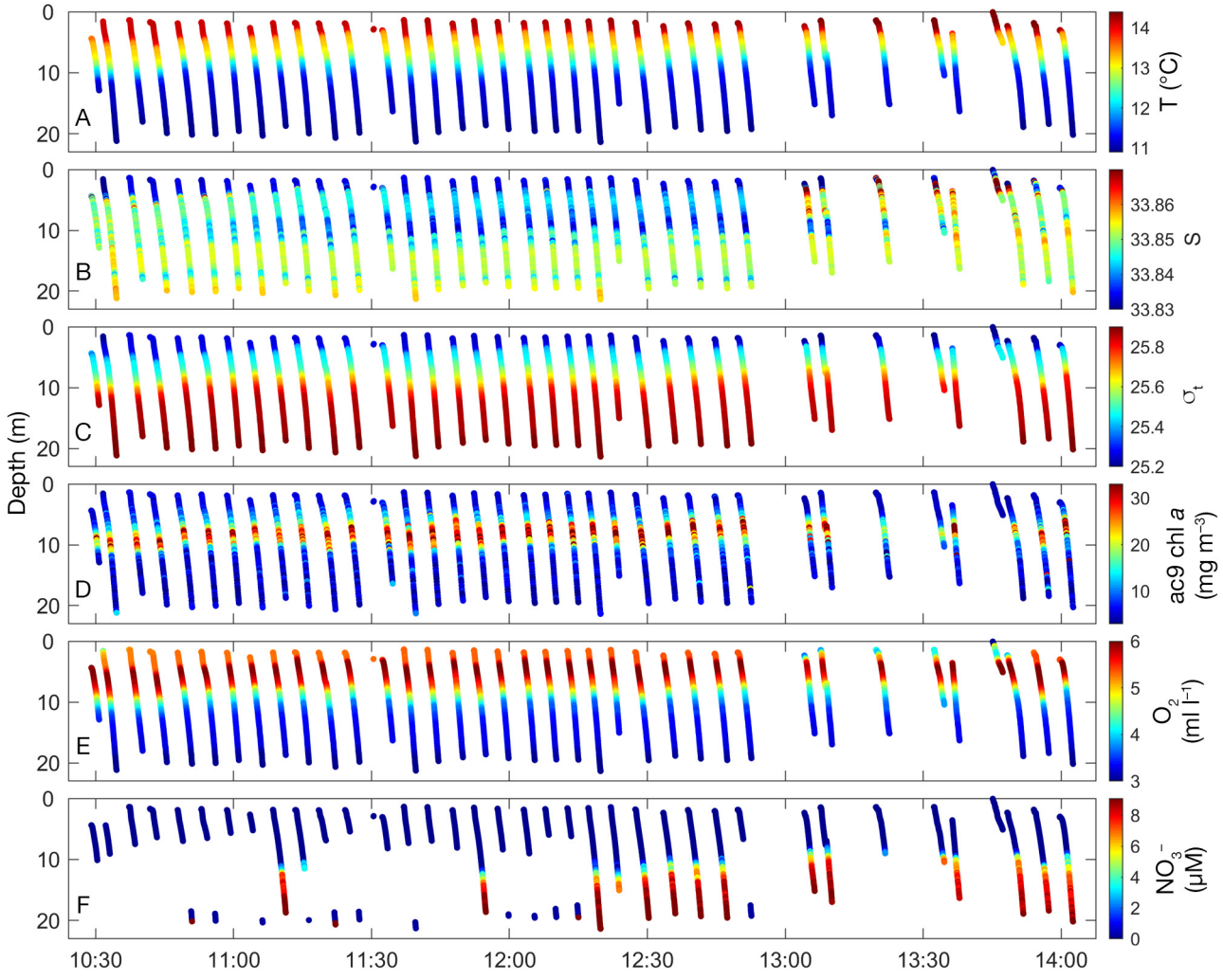

Fig. 4. (A) Temperature (°C), (B) salinity, (C) density (σ_t), (D) ac-9 chlorophyll *a* (mg m^{-3}), (E) oxygen (ml l^{-1}), and (F) nitrate (NO_3^-, µM) sampled with the high-resolution profiler between 10:29 and 14:02 h on 5 July 2010. There were some bad ISUS nitrate-sensor data from a loose/bad electrical connection. These bad data were removed, leading to some gaps in the nitrate data

depth ranged from 7.61 to 10.62 m (9.20 m average).

A thin subsurface layer of elevated chl *a* concentration (chl *a* calculated from the ac-9 measurements, cf. Eq. 1) was positioned at the base of the pycnocline, with an average vertical dimension of 1.16 m (after Dekshenieks et al. 2001) and a range of 0.02–2.76 m. This layer persisted throughout the duration of the profiling (i.e. thin layers were present in 100% of the profiles analyzed) and was positively identified by the layer algorithm in each of the 33 profiles. The peak chl *a* concentration within the layer averaged 57.82 mg m^{-3}, more than 5 times the average background with a range between 37.78 and 191.14 mg m^{-3}. The chl *a* maximum averaged 8.36 ± ~1.5 m in depth (Fig. 4).

Oxygen levels near the surface (<3 m) averaged 4.8 ml l^{-1}. There was a distinct oxygen maximum at 5 m (average O_2 = 5.9 ml l^{-1}), followed by a steep oxycline. The base of the oxycline was co-located with the lower extent of the chl *a* layer.

Nitrate levels in the surface mixed layer remained low (0.18 µM), while elevated nitrate was measured as high as 12.64 µM at 15.2 m, below the pycnocline.

3.3. Bottle samples

Bottle samples were collected within, above, and below the ac-9 chlorophyll layer. This corresponded to depths of 7.4, 4.0, and 15.2 m, respectively, at the time of sampling (13:08, 13:22, 13:36 h on 5 July).

Results for phytoplankton, bacteria and photosynthetic eukaryotes, nutrients, as well as TSS bottle samples are given in the following sections.

3.3.1. Phytoplankton

Pseudo-nitzschia spp. were the most abundant phytoplankton within the thin layer (Table 2). *Pseudo-nitzschia* spp. were 2.8 times higher in the layer compared to above, and 3.1 times higher in the layer compared to below. *P. australis* and *P. multiseries* were present but were not the dominant *Pseudo-nitzschia* spp. However, both dDA and pDA were highest within the layer compared to above and below (Table 2). The pDA per cell was elevated in the thin layer (3.5 pg pDA cell^{-1}) compared to above and below the layer, (1.2 and 2.1 pg pDA cell^{-1}, respectively). While the dominant species in the samples were *Pseudo-nitzschia* spp., all samples also contained *Chaetoceros* spp.. In addition, samples in the thin layer also contained *Lauderia* spp. and *Guinardia* spp.

Table 2. Average (SD) *Pseudo-nitzschia* spp. counts, dissolved domoic acid (dDA), particulate domoic acid (pDA), and calculated pDA cell^{-1} from bottle samples taken at depths of 4.0, 7.4, and 15.2 m

Depth (m)	10^6 cells l^{-1}	dDA µg l^{-1}	pDA µg l^{-1}	pg pDA cell^{-1}
4.0	1.4 (0.5)	0.34 (0.59)	1.66 (0.41)	1.2 (0.5)
7.4	3.9 (1.3)	6.89 (2.83)	13.59 (4.45)	3.5 (1.6)
15.2	1.3 (0.4)	4.98 (3.28)	2.62 (0.57)	2.1 (0.7)

Table 3. Counts of unpigmented bacteria, *Prochlorococcus* spp., *Synechococcus* spp., and photosynthetic eukaryotes from bottle samples taken at depths of 4.0, 7.4, and 15.2 m

Depth (m)	Unpigmented bacteria (10^9 cells l^{-1})	*Prochloro-coccus* (10^7 cells l^{-1})	*Synecho-coccus* (10^7 cells l^{-1})	Photosynthetic eukaryotes (10^6 cells l^{-1})
4.0	3.3	1.7	1.4	5.0
7.4	1.3	1.5	0.58	3.5
15.2	0.40	1.4	0.23	1.5

3.3.2. Bacteria and small photosynthetic eukaryotes

Unlike the diatoms described previously, concentrations of unpigmented bacteria (0.4–3.3 × 10^9 l^{-1}), the photosynthetic bacteria *Prochlorococcus* (1.4–1.7 × 10^7 l^{-1}) and *Synechococcus* (0.23–1.4 × 10^7 l^{-1}), and small photosynthetic eukaryotes (1.5–5.0 × 10^6 l^{-1}) were all most abundant at the surface and their concentrations decreased with depth (Table 3). The decline in *Prochlorococcus* spp. with depth was minimal, but other microbial cells declined 2- to 3-fold at each successively deeper depth.

3.3.3. Nutrients

Concentrations of dissolved inorganic nutrients (NO_3^-, NO_2^-, NH_4^+, PO_4^{3-}, $Si(OH)_4$) were lowest at the surface and increased with depth (Table 4). At the shallowest sampled depth, silica was >1 µM, but inorganic N and P were especially depleted. All inorganic sources of N (NO_3^-, NO_2^-, NH_4^+) at 4 m totaled to 0.27 µM, and P concentration was 0.14 µM for a dissolved inorganic nitrogen to dissolved inorganic phosphorus (DIN:DIP) ratio of 2. In the thin layer (7.4 m), combined inorganic N sources were 10 times higher than at the surface (2.7 µM) and inorganic P was 2-fold higher (0.27 µM), and the DIN:DIP ratio increased to 10. Relative to the within the layer, both inorganic N and P were 6 times higher below the layer (15.2 m), and the inorganic DIN:DIP ratio remained unchanged.

TDN concentration was 10.7 µM both above and in the layer, and increased to 25 µM below the layer. TDP was similar above and within the layer (0.4 and 0.53 µM) and increased to 1.8 µM below. This resulted in the TDN:TDP ratios of 25 above, 20 within, and 14 below the layer.

Table 4. Concentrations of inorganic and total dissolved nutrients (µM), the ratios of dissolved inorganic N and P (DIN:DIP) or total dissolved N and P (TDN:TDP), and the concentration of cell-associated alkaline phosphatase activity (APA; nM P h^{-1}) at 3 depths. DIN was calculated as the sum of the 3 DIN species

Depth	NO_3	NO_2	NH_4	PO_4	$Si(OH)_4$	DIN:DIP	TDN	TDP	TDN:TDP	APA
4.0	0.18	0.01	0.08	0.14	1.24	1.90	10.73	0.43	24.9	3.22
7.4	2.29	0.07	0.34	0.27	1.91	10.00	10.70	0.53	20.2	1.56
15.2	12.64	0.23	3.62	1.58	16.63	10.00	25.01	1.79	13.9	1.87

Bulk APA in the surface water above the layer (3 nM P h^{-1}) was 2 times higher than in or below the layer, but chlorophyll-normalized APA was 8.5 times higher than within the layer and 2.9 times higher than below the layer (Table 4).

3.3.4. TSS

TSS were highest within the layer (11.91 mg l^{-1}) compared to above (7.98 mg l^{-1}) and below the layer (7.33 mg l^{-1}). This is likely also capturing phytoplankton biomass because TSS was only dried and not combusted, thus organics were not removed.

3.4. Towed and shipboard systems

3.4.1. ISIIS

The ISIIS data allow us to compare the particle size and shape distribution to the thin subsurface layer of chl *a* on 5 July between 12:32 and 14:14 h. A total of 931 065 image segments with ESDs >3.3 mm were extracted from the images; a subset of 2000 showed that 96.3% of these segments contained marine snow. The high concentrations of particles across the different size classes overlapped spatially with the area of high chl *a* fluorescence; however, there were some slight differences among the size classes (Fig. 5). The abundance peak of large particles was broader in vertical dimension/extent than the medium and small particle abundance peaks. The spatial locations of the peak concentrations were also different among the groups. Small particles tended to be most abundant in the inshore ends of the transects. Medium-sized particles were most abundant in the middle of the transects but generally had a more horizontally dispersed distribution relative to the other size classes. The large particles were concentrated in a thin layer in the offshore ends of the transects.

The shape of particles within the different size classes varied vertically (Fig. 6). Near the surface, particles from all size classes had a more elongate shape (higher aspect ratio), indicating sinking. The shape of particles within the layer (and below) was more round (lower aspect ratio). Above and below the layer, the large and medium particles were similar in concentration; however, inside the layer, large particles were approximately twice the concentration of the medium size class. It is important to note that the size ranges selected were based on the environment and organisms that were sampled. Our main goal was to distinguish the average particles from the exceptionally large aggregates that were present in the thin layer. The small and medium size categories are exactly 3000 pixels each: 2000–5000, and 5001–8001, respectively. The large category contains the large aggregates from the thin layer — we did not want an upper limit for these. Thus, the size classes small, medium, and large are relative terms.

Particles from 3 discrete areas of the water column showed differences in several measured properties (Fig. 6, Table 5). Concentrations of particles in the thin layer were enhanced 2.28 times relative to concentrations above the layer and 10.26 times relative to concentrations below the layer. The mean area (size) of each particle was enhanced 2.27 times relative to the mean area above the thin layer, and 1.74 times relative to the mean area below the thin layer. The ESD of particles in the thin layer was 1.51 times larger than the ESD of particles above the thin layer, and 1.32 times larger than the ESD of particles below the thin layer. We found that although the aspect ratio of the particles within the layer was low, the perimeter:area ratio was significantly higher than the other sections, indicating that the particles within the layer were large, round, and had an irregular border, which is supported by Fig. 6. The ratio of perimeter: area of particles in the thin layer was 1.11 times higher in the thin layer than above the layer, and 1.36 times higher in the thin layer than below the layer. The aspect ratio reveals that particles near the surface were more elongate, most likely comet-shaped based on observations; this is supported by Fig. 6. Finally, the angle shows that in general, the particles within the layer were relatively more horizontally oriented (angled further from 90°) (Fig. 6, Table 5).

3.4.2. Acoustics

The spatial distribution of acoustic backscatter from the Simrad EK60 split-beam echosounder with a 200 kHz transducer shows an intense subsurface scattering layer that extends for kilometers in the study area (Fig. 7).

Qualitative comparisons were made between single ascending profiles from the ISIIS, and the acoustics averaged over the time of the ISIIS profile (Fig. 8). This example shows increases in particles m^{-3} from the ISIIS, concurrent with acoustic scattering from the Simrad EK60 where the aggregates of marine snow and zooplankton were located. In this profile, there were predominantly copepods just

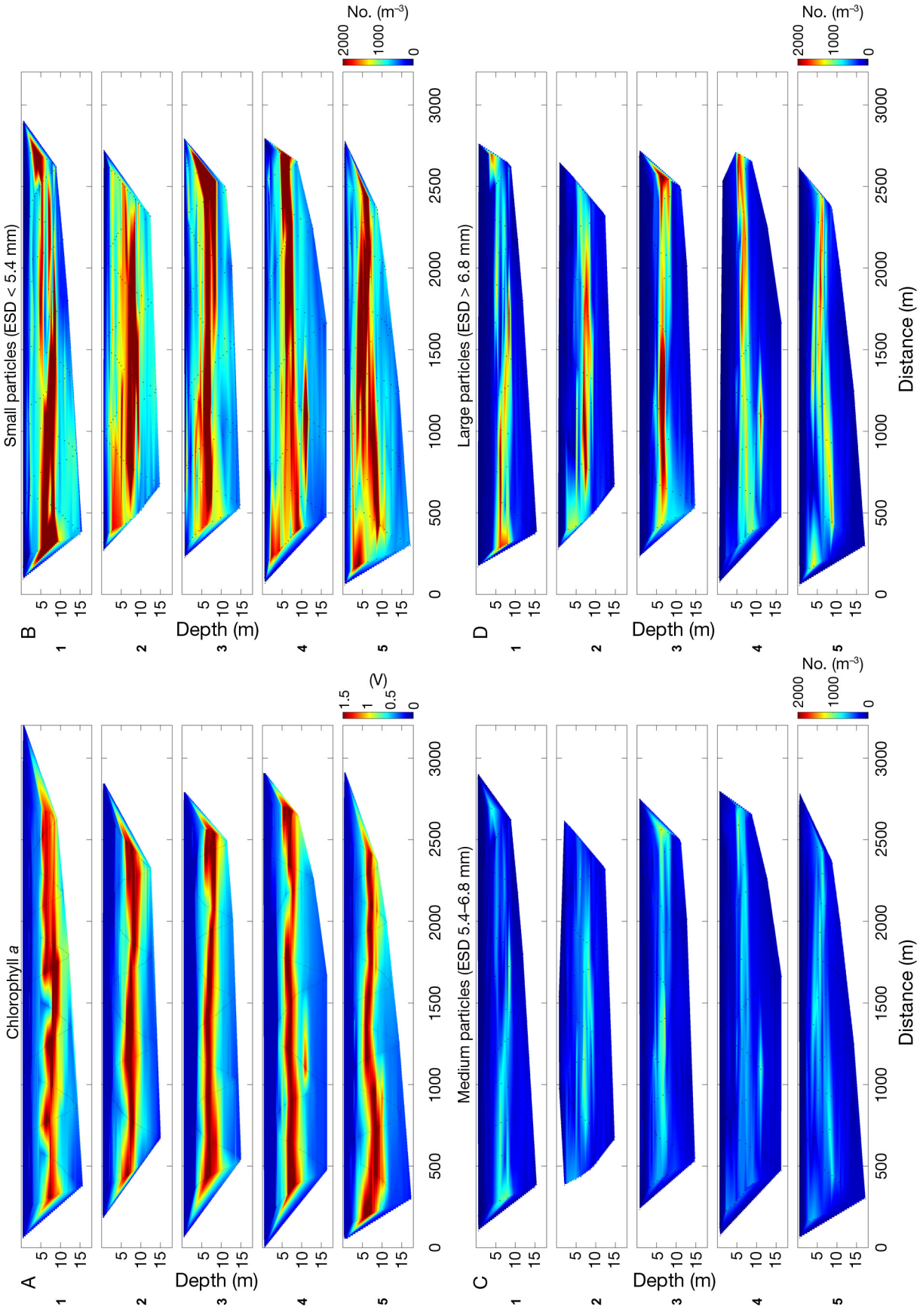

Fig. 5. (A) Chlorophyll *a* (V), (B) small particle aggregates (marine snow) particles (equivalent spherical diameter, ESD <5.4 mm) (no. m^{-3}), (C) medium particles (ESD 5.4–6.8 mm) (no. m^{-3}), and (D) large particles (ESD >6.8 mm) (no. m^{-3}) measured with the *in situ* ichthyoplankton imaging system (ISIIS) on 5 July 2010 between 12:32 and 14:14 h. Numbers 1–5 correspond to acoustic/ISIIS transect numbers in Figs. 1 & 7

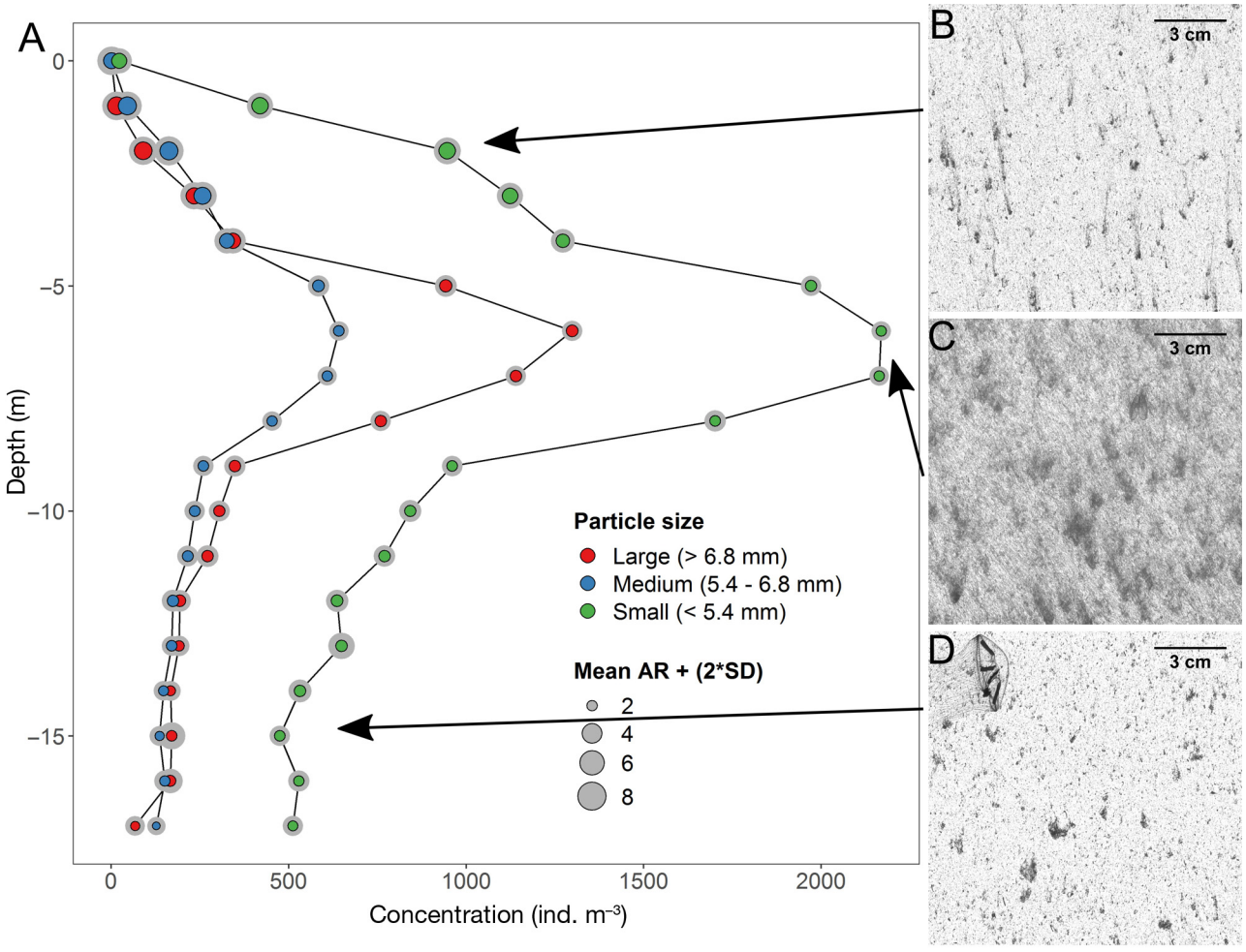

Fig. 6. (A) Average particle size from the *in situ* ichthyoplankton imaging system (ISIIS) vs. mean concentration per 1 m depth bin over all 5 transects. The size of the points corresponds to the mean aspect ratio (AR) per depth bin. Gray circles represent 2 SD of the mean. The AR changes for each size class and the variability within each sample bin. If the gray circle is large relative to the colored dot, this indicates there was high AR variation within the sample bin. Also shown are ISIIS images of particles (B) above, (C) within, and (D) below the thin layer

Table 5. Particle statistics. Equivalent spherical diameter (ESD), perimeter to area ratio of a particle, aspect ratio, and mean angle of orientation in depth ranges above, within, and below the thin layer. An ANOVA was performed with a Tukey's HSD post hoc test for differences among the 3 groups. Groups with significant differences are denoted by '*'

	Location relative to thin layer		
	Above	Within	Below
Depth (m)	2.0–3.0	6.5–7.5	14.0–15.0
ESD (mm)	5.47	8.24	6.24
Perimeter:area ratio	0.207*	0.229*	0.169*
Aspect ratio	3.090*	2.044	2.065
Mean angle of orientation (0–90°)	62.749	56.114	67.140

above and below the layer, and jellies below layer (Fig. 8).

4. DISCUSSION

4.1. Environmental conditions

The environmental conditions in northeastern Monterey Bay on 5 July 2010 were optimal for the development of an intense thin layer. Following 6 d of significant upwelling, where cold nutrient-rich water was upwelled

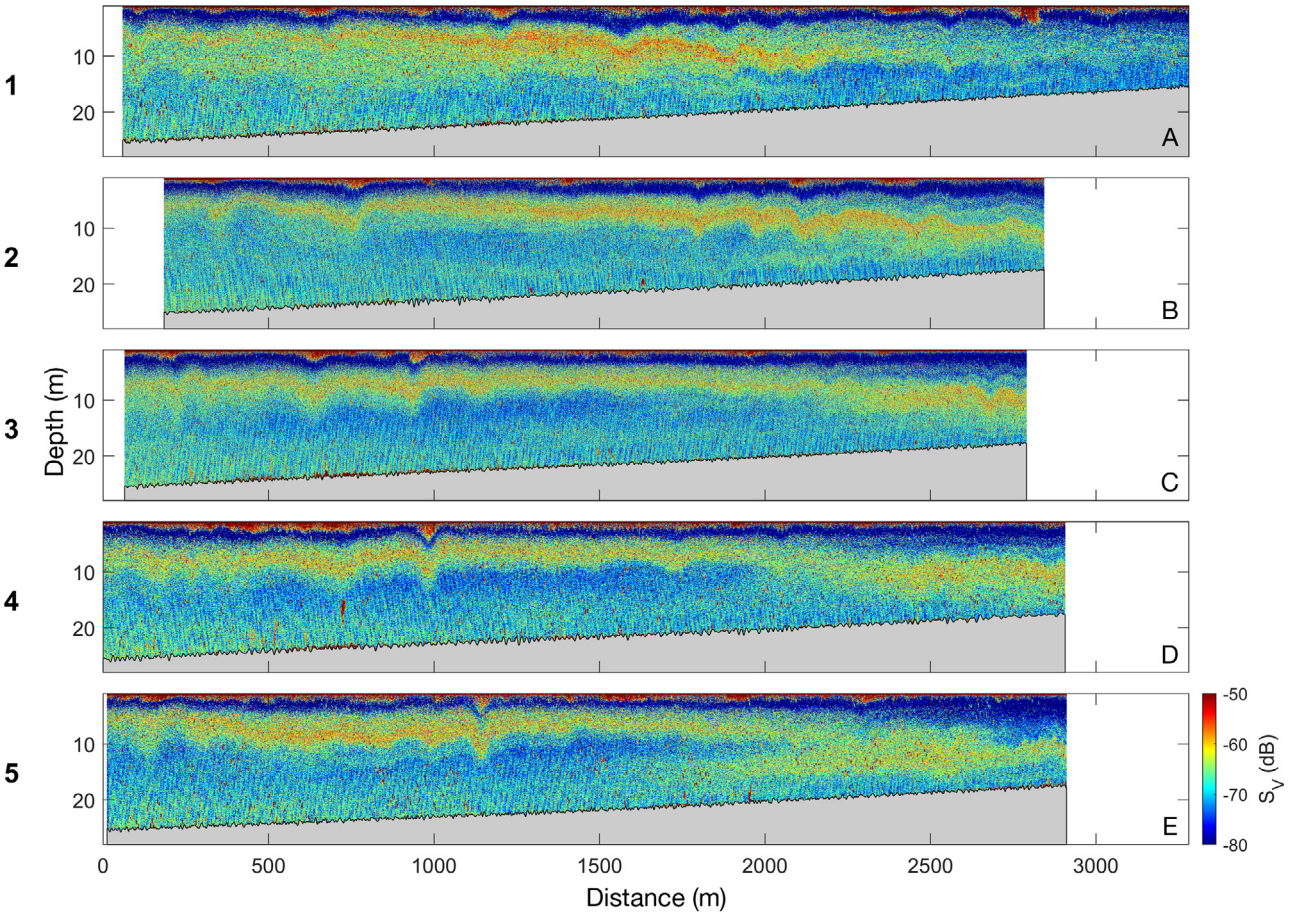

Fig. 7. Acoustic backscatter from the shipboard Simrad EK60 split-beam echosounder with a 200 kHz transducer on 5 July 2010. Gray shading is bathymetry. Numbers 1–5 correspond to acoustic/ISIIS transect numbers in Figs. 1 & 5

to the north of Monterey Bay, 5 July had relatively weak winds from the south and a relaxation from upwelling. Strong stratification in northeastern Monterey Bay was maintained due to a neap tide that reduced tidal range. The period was also characterized by relatively low current velocities, low winds and waves, as well as decreased air temperature fluctuations.

4.2. Phytoplankton

The average vertical dimension of the thin layer was 1.16 m, with a range of 0.02–2.76 m. Previous studies in Monterey Bay have measured thin phytoplankton layers with similar dimensions: McManus et al. (2008) measured thin layers in northeastern Monterey Bay ranging in thickness from 0.10 to 3.0 m, with 85% of thin layers <2 m and 54% of thin layers <1 m; Ryan et al. (2008) measured thin layers in eastern Monterey Bay averaging 2.3 m; Ryan et al. (2010) measured thin layers across Monterey Bay with an average thickness of 1.4 m; and Timmerman et al. (2014) found that the average thickness of thin layers in northeast Monterey Bay was 2.4 m. Previous studies in East Sound, Washington, have also found comparable dimensions. Over 3 mo of sampling in 1996, Dekshenieks et al. (2001) found that the average vertical dimension of thin layers was 1.20 m, with a range of 0.12 to 3.61 m. Interestingly, layers measured in oligotrophic tropical waters are thinner and more ephemeral. McManus et al. (2012) found that the average vertical dimension of thin layers in the coastal waters off O'ahu, Hawai'i, was 0.67 m, with a range of 0.21 to 1.29 m. This difference is likely due to the relatively lower levels of stratification and nightly convective overturning occurring in these tropical waters.

Previous observations from this northeast corner of Monterey Bay, California, indicate that thin layers of

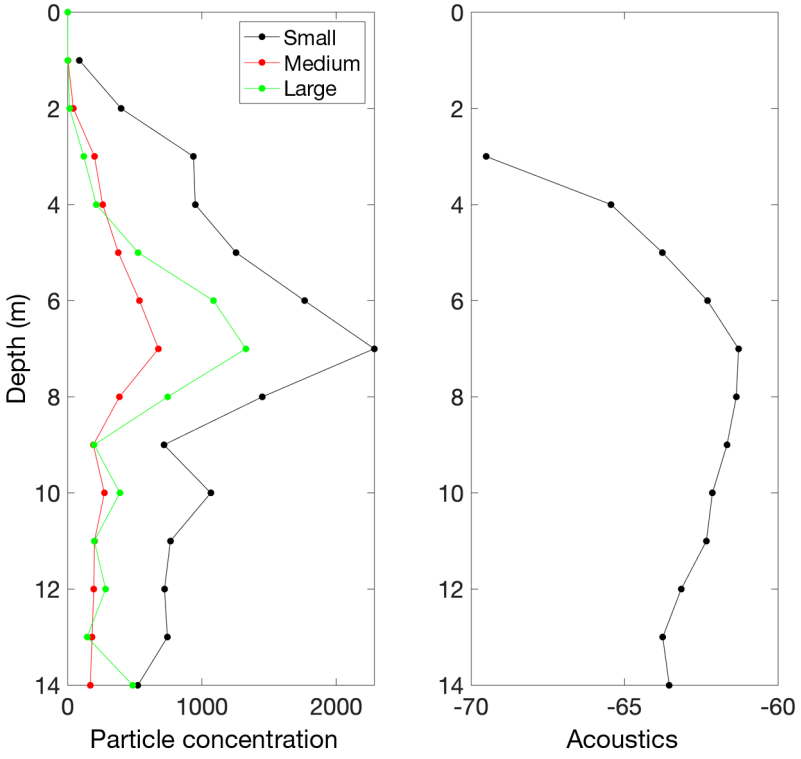

Fig. 8. (A) Particle concentration (m^{-3}) from a single ascending profile of the *in situ* ichthyoplankton imaging system (ISIIS), for small (black), medium (red), and large (green) particles (as defined in Fig. 5). (B) Acoustic backscatter (dB) from the Simrad EK60 split-beam echosounder with a 200 kHz transducer

HAB species, such as *Pseudo-nitzschia* spp., are regular features here (McManus et al. 2008, Ryan et al. 2014, Timmerman et al. 2014), further underscoring the need for subsurface, fine-scale sampling techniques for effective HAB monitoring.

4.3. Suspended sediment

Ryan et al. (2014) suggested that small-scale heterogeneity in the toxicity of *Pseudo-nitzschia* spp. populations in thin layers in Monterey Bay was related to the coupling of resuspended sediments from the bottom boundary layer to the surface mixed layer. It is possible that resuspended sediments from the bottom boundary layer were entrained in the pycnocline during the wind mixing events observed between 29 June and 4 July. Even though other instruments may have been able to detect these suspended sediments, the suspended sediment would be below the size threshold for ISIIS detection (~3.3 mm ESD) and would likely not form aggregates, as is common with coalesced particles of biological origin (e.g. Burd & Jackson 2009).

4.4. Nutrients, N:P ratio, APA, and domoic acid

The very low (sub-micromolar) inorganic N and P concentrations observed in the surface water suggest that the dissolved organic nutrient reservoirs (which comprise the majority of TDN and TDP in the surface) could be an important resource for phytoplankton. The relative depletion of dissolved P above and within the layer — with TDN:TDP ratios above the canonical Redfield ratio of 16 — suggests that phosphorus stress could be driving selective remineralization of P from dissolved organic sources. This is also supported by the significantly elevated APA in the surface waters. APA has been employed as a proxy for P stress in phytoplankton (Dyhrman & Palenik 1999, Dyhrman & Ruttenberg 2006, Ou et al. 2006), but may also reflect other physiological stresses (Fuentes et al. 2014). Heterotrophic bacteria also express phosphatase (Martinez et al. 1996, Hoppe 2003), so the APA in total community measurements (>0.2 µm fraction), as done here, cannot be ascribed solely to phytoplankton. Nevertheless, the elevated APA, low inorganic P concentration, and high TDN:TDP ratio in the surface water suggest phytoplankton would have been P stressed.

Phosphorus stress can have a significant influence on *Pseudo-nitzschia* growth and domoic acid production. In a chemostat experiment using *P. multiseries*, Hagström et al. (2011) showed that P deficiency occurred when the cellular ratio was >14.7, and phosphorus limitation has been found to increase domoic acid production (Lema et al. 2017, Hagström et al. 2011). Given the low inorganic N concentrations in the surface water, and an inorganic DIN:DIP ratio of 2, it seems likely that the diatoms in the surface waters will also face some degree of N stress. This would contribute to lower concentrations of cells by reducing growth and possibly stimulate aggregation and sinking as marine snow (Sekula-Wood et al. 2009, Schnetzer et al. 2017), and could also limit domoic acid production, a nitrogen-containing compound (Bates et al. 1991).

The non-proportional increase in nutrients observed in the thin layer could relieve N limitation for

diatoms either growing at that depth or arriving in sinking aggregates. According to physiological modeling efforts (Terseleer et al. 2013), the elevated N (2.3 µM) in the layer could, given sufficient light, trigger significant increases in domoic acid production. This is consistent with our observations that particulate domoic acid per cell is elevated in the thin layer compared to above and below the layer. Inorganic P remains low in absolute terms (0.27 nM) in the layer, and the TDN:TDP ratio remains high, yet APA is low. Perhaps an increased rate in the supply of P across the pycnocline suppresses APA. The exceptionally low chl *a*-normalized APA suggests that the diatoms are not the major source of APA in the thin layer. Accordingly, we propose a scenario in which phosphorus (and perhaps nitrogen) stress above the thin layer may contribute to the aggregation and sinking of *Pseudo-nitzschia* spp., while a disproportionate increase in N availability in the layer may increase toxicity of cells that accumulate there.

4.5. Bacteria

In the California Bight, Collier & Palenik (2003) found that *Synechococcus* had the highest concentration in the mixed layer and decreased with depth, similar to our study. Further, they found that in areas influenced by upwelling, *Synechococcus* and chl *a* had an inverse relationship, supporting that higher abundance is not necessarily within the layer. Observations from our study site in June and August 2010 also found that *Synechococcus* abundance was more variable and had higher concentrations at lower chl *a* concentrations (Timmerman 2012).

4.6. Particle size distribution measured with *in situ* imaging

Complementary to other biological, physical, and chemical measurements, *in situ* imaging allowed for automated detection and sizing of particles/plankton in and around the thin layer that indicate how thin layers form. While automated image classification algorithms were not used in this study, a random sample of the over 900 000 segments extracted during the 5 transects revealed that >96% of particles larger than the 3.3 mm ESD size threshold were marine snow (aggregates). Even in more oligotrophic systems relative to Monterey Bay, detritus forms >90% of particles imaged with optical systems (Laser Optical Plankton Counter; Espinasse et al. 2018). The particle aggregates imaged with the ISIIS are easily identified by eye because the particles are dark, irregular in shape, and do not include an organism in the meso- to macro-zooplankton size range. Particle aggregates can, however, vary greatly in size and shape, information which can be extracted automatically and indicate physical processes contributing to vertical flux (i.e. elongated and vertically oriented, indicating sinking).

The particle aggregates in the study had several quantifiable properties indicating how the layer was formed and persisted through time and space. All 3 size classes of particles were most abundant within the thin layer, corresponding to the area of high chl *a* fluorescence. Because the particles were more elongated above the layer and changed orientation angle (and increased in size) within the layer, this suggests passive accumulation of particles along a physical gradient similar to mechanisms described previously (Alldredge et al. 2002, Prairie et al. 2013, 2015). Shear can also contribute to thin layer formation (Ryan et al. 2008, Sevadjian et al. 2014), and the shift in marine snow orientation angle near the pycnocline suggests that shear may have played a role for the thin layer described in this study. A similar pattern above the thin layer was described by Timmerman et al. (2014), who sampled the same region on 27 June 2010, observing that particles above the thin layer were elongated, which they attributed to sinking.

Although several zooplankton groups were conspicuously absent within the thin layer (e.g. these groups were observed to aggregate immediately above and below as in Greer et al. 2013), particle abundance and acoustic backscatter both peaked within the thin layer. Individual aggregates can produce acoustic backscatter signals at very high frequencies (1.5–2.5 MHz; Briseño-Avena et al. 2018), but these aggregates are different in both shape and density compared to the continuous layer of phytoplankton aggregates (dominated by diatoms) found inside the thin layer and described here. Particle aggregates have been shown to accumulate at density gradients in a variety of ocean systems, and the component that is phytoplankton likely contributes to chl *a* signals (Greer et al. 2015, Graff & Menden-Deuer 2016, Bochdansky et al. 2017).

Zooplankton have been shown to avoid patches of potentially toxic phytoplankton (Fiedler 1982, Talapatra et al. 2013). Greer et al. (2013) observed that copepods have a bi-modal vertical distribution and appeared to avoid the thin layer on multiple days of sampling. It seems reasonable that zooplankton

would avoid a layer of 'stressed' diatoms that were producing domoic acid. Similar distributional patterns were observed in the Gulf of Mexico, where copepods were not common inside a thin layer of diatom chains (primarily *Odontella* sp.), but instead aggregated near the surface outside of the layer (Greer et al. 2020). The diatoms in the northern Gulf of Mexico thin layer, however, did not form distinct clumps or aggregates but rather formed a large 'mat' (i.e. in the Gulf of Mexico study, particle counting was not possible inside the layer because there were no distinct aggregates). Despite the differences in appearance of the layer in the imagery, the general avoidance of the layer by copepods was consistent between the studies. It is important to note that lack of grazing can also enhance a thin layer.

Other zooplankton groups may be abundant inside the layer due to their ecological preferences or passive accumulation. Doliolids (pelagic tunicates) were one of the most abundant mesozooplankton groups in the northern Gulf of Mexico and were concentrated inside the thin layer (Greer et al. 2020). Pelagic tunicates were rare or absent during our study in Monterey Bay, although other gelatinous species that may sometimes consume phytoplankton were found within the layer in much lower abundances relative to copepods (e.g. *Bolinopsis* spp. ctenophores, Greer et al. 2013).

There were some slight differences among the size classes measured by the ISIIS (Figs. 6 & 7). The largest size class of particles has a relatively narrow vertical extent compared to the medium and small sizes. The horizontal spatial locations of the peak concentrations also differed among the groups. The limited vertical extent of the largest particles is consistent with findings that particle collisions and aggregation through transparent exopolymers (TEPs, components of the broader pool of extracellular polymeric substances; Thornton 2002) that increase 'stickiness', should occur rapidly within a narrow pycnocline (Passow & Alldredge 1994, Passow 2002, Prairie et al. 2013, Tréguer et al. 2018). It is possible that TEP abundance in the thin layer might contribute to increased viscosity in the layer and that would be less desirable to grazers leading to crustacean zooplankton (i.e. copepods) avoiding the thin layer.

The distribution of TEPs was not measured in this study but likely plays an important role in the formation of thin layers and conceptually links the measurements from our different sampling systems. These polysaccharides form the 'glue' that can cause aggregations of phytoplankton, bacteria, and other particles (Passow 2002, Burd & Jackson 2009). High amounts of TEPs are often positively correlated with chl *a*, and can result in the formation of large 'mats' of diatoms, bacteria, and suspended sediment that do not sink (or do so very slowly) (Passow 2002).

TEP production tends to increase as phytoplankton growth rates decrease (Engel et al. 2002), and this could be tied to physiological stress in both phytoplankton (Moriceau et al. 2007, Kahl et al. 2008) and microbes (Quigg et al. 2016). The TDN:TDP ratios in the upper water column, which displayed a substantial departure from Redfield ratios, and overall high abundances of microbes indicate that nutrient stress may have played a role in generating TEP production (from both phytoplankton and microbes), serving as the adhesive mechanism forming the comet-shaped flocs imaged by the ISIIS (Fig. 6). The formation of flocs is species dependent. For example, Passow et al. (2019; p. 73, their Table 3) noted that *Chaetoceros* spp. took a relatively long time to form aggregates, and once formed, they tended to be 'wispy and stringy' with few solid particles. Morphologically, the aggregates measured in our study were large and solid, similar to ones found for *Odontella* (Passow et al. 2019). As large, chain-forming diatom species, it is reasonable to expect *Pseudo-nitzschia* spp. to form similar large aggregates. These aggregates then settled to the pycnocline to form the thin layer (e.g. Prairie et al. 2013).

The timing of sampling could be critical for influencing the properties of the layer, as Greer et al. (2020) described a thin layer in the northern Gulf of Mexico primarily composed of healthy *Odontella* sp. diatoms with few large flocs. The layer in the northern Gulf of Mexico, in contrast to the one we described in Monterey Bay, had a strong peak in oxygen that was spatially co-located with the chl *a* fluorescence peak, indicating photosynthesis outweighing respiration within the layer. On the other hand, thin layers of marine snow aggregates or flocs with decaying oxygen concentrations inside the thin layer indicate that respiration dominates over any photosynthetic processes, with chlorophyll still high but lower dissolved oxygen. These differences in the spatial relationships between dissolved oxygen and chl *a* may have been related to the physical mechanisms of thin-layer formation. The thin layer in the northern Gulf of Mexico was likely formed by a surface convergence combined with diatom buoyancy (Greer et al. 2020) as opposed to the passive settling mechanism with limited shear well described in Monterey Bay (Graham & Largier 1997, Prairie et al. 2013). These differences in physical forcing driving

thin-layer formation may also influence some of the differences in the appearance of the marine snow in the imagery.

Future studies following our sampling scheme may want to add measurements of TEPs, as these substances can be important for entraining and concentrating sediments (Fabricius & Wolanski 2000), as well as oil and other pollutants (Ladd et al. 2018, Passow et al. 2019).

5. CONCLUSIONS

An intense, persistent thin layer of phytoplankton was observed in northeastern Monterey Bay on 5 July 2010. The average vertical dimension of the thin layer was 1.16 m, which is similar to other studies in highly stratified coastal systems. The majority of the phytoplankton in the thin layer comprised *Pseudo-nitzschia* spp., and several zooplankton groups were observed immediately above and below the layer. Over 96% of particle aggregates in the thin layer were larger than the 3.3 mm ESD size threshold. Because the particles were more elongated above the layer and changed orientation angle (and increased in size) within the layer, this suggests passive accumulation of particles along a physical gradient. Further, the shift in particle orientation angle near the pycnocline suggests that shear may have played a role for the thin layer described in this study. The limited vertical extent of the largest particles is consistent with findings that particle collisions, and aggregation through TEPs that increase 'stickiness', should occur rapidly within a narrow pycnocline. The distribution of TEPs was not measured in this study but likely plays an important role in linking the measurements from different sampling systems. TEP production tends to increase as phytoplankton growth rates decrease, and this could be tied to physiological stress in both phytoplankton and microbes. We suggest that phosphorus (and perhaps nitrogen) stress above the thin layer may contribute to the aggregation and sinking of *Pseudo-nitzschia* spp., while a disproportionate increase in N availability in the thin layer may increase toxicity of cells that accumulate there. With the knowledge that HAB events can occur subsurface, modified sampling methods to monitor for these hidden incubators could greatly improve the efficacy of early-warning systems designed to detect HABs in coastal waters.

As more thin layers are described in different ecosystems, comparisons of physical forcing, species composition, as well as distributions of nutrients and higher trophic levels will be critical information for understanding the potential trophic impacts of thin layers in marine ecosystems. This information will be increasingly important as marine systems change with rising average global temperatures and other sources of anthropogenic influence.

Acknowledgements. We thank G. Steward for detailed editing of the manuscript, K. Selph for assistance with bacterial analyses, J. Sullivan for helpful discussion regarding the ac-9, K. Ruttenberg for assistance with the nutrient sampling plan, R. Kudela for assistance with domoic acid, as well as boat captains Jim Christmann of the 'Shana Rae' and John Douglas of the 'Sheila' (Moss Landing Marine Laboratory). We thank R. K. Takesue from USGS, the Associate Managing Editor and Contributing Editor of MEPS, as well as 3 anonymous reviewers for their constructive and helpful comments on the manuscript. The research described here is based upon work supported by the National Science Foundation Graduate Research Fellowship under Grant no. DGE-0822443 (A.H.V.T.), National Science Foundation Research Grant no. OCE-0925916 Lateral Mixing (M.A.M.), and National Science Foundation RAPID Grant no. OCE-1035047 (R.C.). Any use of trade, firm, or product names is for descriptive purposes only and does not imply endorsement by the US Government.

LITERATURE CITED

Alldredge AL, Cowles TJ, MacIntyre S, Rines JEB and others (2002) Occurrence and mechanisms of formation of a dramatic thin layer of marine snow in a shallow Pacific fjord. Mar Ecol Prog Ser 233:1–12

Bates SS, de Freitas ASW, Milley J, Pocklington R, Quilliam MA, Smith JC, Worms J (1991) Controls on domoic acid production by the diatom *Nitzschia pungens* f. *multiseries* in culture: nutrients and irradiance. Can J Fish Aquat Sci 48:1136–1144

Bennett AF, Denman KL (1985) Phytoplankton patchiness: inferences from particle statistics. J Mar Res 43:307–335

Benoit-Bird KJ, McManus MA (2012) Bottom-up regulation of a pelagic community through aggregations. Biol Lett 8:813–816

Berdalet E, McManus MA, Ross ON, Buchard H and others (2014) Understanding harmful algae in stratified systems: review of progress and future directions. Deep Sea Res II 101:4–20

Bjørnsen PK, Nielsen TG (1991) Decimeter scale heterogeneity in the plankton during a pycnocline bloom of *Gyrodinium aureolum*. Mar Ecol Prog Ser 73:263–267

Bochdansky AB, Clouse MA, Hansell DA (2017) Mesoscale and high-frequency variability of macroscopic particles (>100 µm) in the Ross Sea and its relevance for late-season particulate carbon export. J Mar Syst 166: 120–131

Briseño-Avena C, Franks PJS, Roberts PLD, Jaffe JS (2018) A diverse group of echogenic particles observed with a broadband, high frequency echosounder. ICES J Mar Sci 75:471–482

Burd AB, Jackson GA (2009) Particle aggregation. Annu Rev Mar Sci 1:65–90

Cheriton OM, McManus MA, Holliday DV, Greenlaw CF, Donaghay PL, Cowles T (2007) Effects of mesoscale

physical processes on thin zooplankton layers at four sites along the West Coast of the US. Estuaries Coasts 30: 575–590

Cheriton OM, McManus MA, Stacey MT, Steinbuck JV (2009) Physical and biological controls on the maintenance and dissipation of a thin phytoplankton layer. Mar Ecol Prog Ser 378:55–69

Cheriton OM, McManus MA, Steinbuck JV, Stacey MT, Sullivan JM (2010) Towed vehicle observations of across-shelf thin layer structure and a low-salinity intrusion in northern Monterey Bay, CA. Cont Shelf Res 30:39–49

Churnside JH, Donaghay PL (2009) Thin scattering layers observed by airborne lidar. ICES J Mar Sci 66:778–789

Clay CS, Medwin H (1977) Acoustical oceanography: principles and applications. John Wiley & Sons, New York, NY

Collier JL, Palenik B (2003) Phycoerythrin-containing picoplankton in the Southern California Bight. Deep Sea Res II 50:2405–2422

Cowen RK, Guigand CM (2008) *In situ* ichthyoplankton imaging system (ISIIS): system design and preliminary results. Limnol Oceanogr Methods 6:126–132

Cowles TJ, Desiderio RA, Carr ME (1998) Small-scale planktonic structure: persistence and trophic consequences. Oceanography 11:4–9

Dekshenieks MM, Donaghay PL, Sullivan JM, Rines JEB, Osborn TR, Twardowski MS (2001) Temporal and spatial occurrence of thin phytoplankton layers in relation to physical processes. Mar Ecol Prog Ser 223:61–71

Donaghay PL, Rines HM, Sieburth JM (1992) Simultaneous sampling of fine scale biological, chemical, and physical structure in stratified waters. Arch Hydrobiol Beih Ergebn Limnol 36:97–108

Dyhrman ST, Palenik B (1999) Phosphate stress in cultures and field populations of the dinoflagellate *Prorocentrum minimum* detected by a single-cell alkaline phosphatase assay. Appl Environ Microbiol 65:3205–3212

Dyhrman ST, Ruttenberg KC (2006) Presence and regulation of alkaline phosphatase activity in eukaryotic phytoplankton from the coastal ocean: implications for dissolved organic phosphorus remineralization. Limnol Oceanogr 51:1381–1390

Engel A, Goldthwait S, Passow U, Alldredge A (2002) Temporal decoupling of carbon and nitrogen dynamics in a mesocosm diatom bloom. Limnol Oceanogr 47:753–761

Espinasse B, Basedow S, Schultes S, Zhou M, Berline L, Carlotti F (2018) Conditions for assessing zooplankton abundance with LOPC in coastal waters. Prog Oceanogr 163: 260–270

Fabricius KE, Wolanski E (2000) Rapid smothering of coral reef organisms by muddy marine snow. Estuar Coast Shelf Sci 50:115–120

Fiedler PC (1982) Zooplankton avoidance and reduced grazing responses to *Gymnodinium splendens* (Dinophyceae). Limnol Oceanogr 27:961–965

Fuentes S, Wikfors GH, Meseck S (2014) Silicon deficiency induces alkaline phosphatase enzyme activity in cultures of four marine diatoms. Estuaries Coasts 37:312–324

Graff JR, Menden-Deuer S (2016) Physical and optical properties of phytoplankton-rich layers in a coastal fjord: a step toward prediction and strategic sampling of plankton patchiness. Mar Ecol Prog Ser 544:1–14

Graham WM, Largier JL (1997) Upwelling shadows as nearshore retention sites: the example of northern Monterey Bay. Cont Shelf Res 17:509–532

Greer AT, Cowen RK, Guigand CM, McManus MA, Sevadjian JC, Timmerman AHV (2013) Relationships between phytoplankton thin layers and the fine-scale spatial distributions of two trophic levels of zooplankton. J Plankton Res 35:939–956

Greer AT, Cowen RK, Guigand CM, Hare JA (2015) Fine-scale planktonic habitat partitioning at a shelf-slope front revealed by a high-resolution imaging system. J Mar Syst 142:111–125

Greer AT, Boyette AD, Cruz VJ, Cambazoglu MK and others (2020) Contrasting fine-scale distributional patterns of zooplankton driven by the formation of a diatom-dominated thin layer. Limnol Oceanogr 65:2236–2258

Hagström JA, Granéli E, Moreira MO, Odebrecht C (2011) Domoic acid production and elemental composition of two *Pseudo-nitzschia multiseries* strains, from the NW and SW Atlantic Ocean, growing in phosphorus- or nitrogen-limited chemostat cultures. J Plankton Res 33: 297–308

Hodges BA, Fratantoni DM (2009) A thin layer of phytoplankton observed in the Philippine Sea with a synthetic moored array of autonomous gliders. J Geophys Res 114: C10020

Holliday DV, Donaghay PL, Greenlaw CF, McGehee DE, McManus MA, Sullivan JM, Miksis JL (2003) Advances in defining fine- and micro-scale pattern in marine plankton. Aquat Living Resour 16:131–136

Hoppe HG (2003) Phosphatase activity in the sea. Hydrobiologia 493:187–200

Hu ZX, Xu N, Li AF, Duan SS (2008) Effects of different N:P ratios on the growth of *Pseudo-nitzschia pungens*, *Prorocentrum donghaiense* and *Phaeocystis globosa*. Shui Sheng Sheng Wu Hsueh Bao 32:482–487

Kahl LA, Vardi A, Schofield O (2008) Effects of phytoplankton physiology on export flux. Mar Ecol Prog Ser 354: 3–19

Ladd TM, Bullington JA, Matson PG, Kudela RM, Iglesias-Rodriguez MD (2018) Exposure to oil from the 2015 Refugio spill alters the physiology of a common harmful algal bloom species, *Pseudo-nitzschia australis*, and the ubiquitous coccolithophore, *Emiliania huxleyi*. Mar Ecol Prog Ser 603:61–78

Lasker R (1975) Field criteria for survival of anchovy larvae: the relation between inshore chlorophyll maximum layers and successful first feeding. Fish Bull 3:453–462

Lema KA, Latimier M, Nézan É, Fauchot J, Le Gac M (2017) Inter and intra-specific growth and domoic acid production in relation to nutrient ratios and concentrations in *Pseudo-nitzschia*: phosphate an important factor. Harmful Algae 64:11–19

Martinez J, Smith DC, Steward GF, Azam F (1996) Variability in ectohydrolytic enzyme activities of pelagic marine bacteria and its significance for substrate processing in the sea. Aquat Microb Ecol 10:223–230

McManus MA, Alldredge AL, Barnard AH, Boss E and others (2003) Characteristics, distribution and persistence of thin layers over a 48 hour period. Mar Ecol Prog Ser 261:1–19

McManus MA, Cheriton OM, Drake PT, Holliday DV, Storlazzi CD, Donaghay PL, Greenlaw CF (2005) Effects of physical processes on the structure and transport of thin zooplankton layers in the coastal ocean. Mar Ecol Prog Ser 301:199–215

McManus MA, Kudela RM, Silver MV, Steward GF, Sullivan JM, Donaghay PL (2008) Cryptic blooms: Are thin layers the missing connection? Estuaries Coasts 31:396–401

McManus MA, Sevadjian JC, Benoit-Bird KJ, Cheriton OM, Timmerman AHV, Waluk CM (2012) Observations of thin layers in coastal Hawaiian waters. Estuaries Coasts 35:1119–1127

Mobley CD, Sundman LK, Boss E (2002) Phase function effects on oceanic light fields. Appl Opt 41:1035–1050

Moriceau B, Garvey M, Ragueneau O, Passow U (2007) Evidence for reduced biogenic silica dissolution rates in diatom aggregates. Mar Ecol Prog Ser 333:129–142

Ou L, Huang B, Lin L, Hong H, Zhang F, Chen Z (2006) Phosphorus stress of phytoplankton in the Taiwan Strait determined by bulk and single-cell alkaline phosphatase activity assays. Mar Ecol Prog Ser 327:95–106

Passow U (2002) Transparent exopolymer particles (TEP) in aquatic environments. Prog Oceanogr 55:287–333

Passow U, Alldredge AL (1994) Distribution, size and bacterial colonization of transparent exopolymer particles (TEP) in the ocean. Mar Ecol Prog Ser 113:185–198

Passow U, Sweet J, Francis S, Xu C and others (2019) Incorporation of oil into diatom aggregates. Mar Ecol Prog Ser 612:65–86

Prairie JC, Ziervogel K, Arnosti C, Camassa R and others (2013) Delayed settling of marine snow at sharp density transitions driven by fluid entrainment and diffusion-limited retention. Mar Ecol Prog Ser 487:185–200

Prairie JC, Ziervogel K, Camassa R, McLaughlin RM, White BL, Dewald C, Arnosti C (2015) Delayed settling of marine snow: effects of density gradient and particle properties and implications for carbon cycling. Mar Chem 175: 28–38

Quigg A, Passow U, Chin W, Xu C and others (2016) The role of microbial exopolymers in determining the fate of oil and chemical dispersants in the ocean. Limnol Oceanogr Lett 1:3–26

Raine R, Berdalet E, McManus MA, Yamazaki H (2014) Harmful algal blooms in stratified systems. Deep Sea Res II 101:1–3

Ryan JP, McManus MA, Paduan JD, Chavez FP (2008) Phytoplankton thin layers caused by shear in frontal zones of a coastal upwelling system. Mar Ecol Prog Ser 354:21–34

Ryan JP, Fischer AM, Kudela RM, McManus MA and others (2010) Recurrent frontal slicks of a coastal ocean upwelling shadow. J Geophys Res Oceans 115:C12070

Ryan JP, McManus MA, Kudela RM, Lara Artigas M and others (2014) Boundary influences on HAB phytoplankton ecology in a stratification-enhanced upwelling shadow. Deep Sea Res II 101:63–79

Schneider CA, Rasband WS, Eliceiri KW (2012) NIH Image to ImageJ: 25 years of image analysis. Nat Methods 9: 671–675

Schnetzer A, Lampe RH, Benitez-Nelson CR, Marchetti A, Osburn CL, Tatters AO (2017) Marine snow formation by the toxin-producing diatom, *Pseudo-nitzschia australis*. Harmful Algae 61:23–30

Scholin CA, Gulland F, Doucette GJ, Benson S and others (2000) Mortality of sea lions along the central California coast linked to a toxic diatom bloom. Nature 403:80–84

Sekula-Wood E, Schnetzer A, Benitez-Nelson CR, Anderson C, Berelson WM, Brzezinski MA (2009) Rapid downward transport of the neurotoxin domoic acid in coastal waters. Nat Geosci 2:272–275

Selph KE, Shacat J, Landry MR (2005) Microbial community composition and growth rates in the NW Pacific during spring 2002. Geochem Geophys Geosyst 6:Q12M05

Sevadjian JC, McManus MA, Pawlak G (2010) Effects of physical structure and processes on thin zooplankton layers in Mamala Bay, Hawaii. Mar Ecol Prog Ser 409: 95–106

Sevadjian JC, McManus MA, Ryan JP, Greer AT, Cowen RK, Woodson CB (2014) Across-shore variability in plankton layering and abundance on the northern Monterey Bay inner shelf. Cont Shelf Res 72:138–151

Strickland JDH (1968) A comparison of profiles of nutrient and chlorophyll concentrations taken from discrete depths and by continuous recording. Limnol Oceanogr 13:388–391

Talapatra S, Hong J, McFarland M, Nayak AR and others (2013) Characterization of biophysical interactions in the water column using *in situ* digital holography. Mar Ecol Prog Ser 473:29–51

Terseleer N, Gypens N, Lancelot C (2013) Factors controlling the production of domoic acid by *Pseudo-nitzschia* (Bacillariophyceae): a model study. Deep Sea Res II 24: 45–53

Thornton DCO (2002) Diatom aggregation in the sea: mechanisms and ecological implications. Eur J Phycol 37: 149–161

Timmerman AHV (2012) Hidden thin layers of toxic diatoms in a coastal bay. MSc thesis, University of Hawaii, Honolulu, HI

Timmerman AHV, McManus MA, Cheriton OM, Cowen RK and others (2014) Hidden thin layers of toxic diatoms in a coastal bay. Deep Sea Research II 101:129–140

Trainer VL, Adams NG, Bill BD, Stehr CM and others (2000) Domoic acid production near California coastal upwelling zones, June 1998. Limnol Oceanogr 45:1818–1833

Tréguer P, Bowler C, Moriceau B, Dutkiewicz S and others (2018) Influence of diatom diversity on the ocean biological carbon pump. Nat Geosci 11:27–37

Wang Z, King KL, Ramsdell JS, Doucette GJ (2007) Determination of domoic acid in seawater and phytoplankton by liquid chromatography–tandem mass spectrometry. J Chromatogr A 1163:169–176

Wickham H (2011) The split–apply–combine strategy for data analysis. J Stat Softw 40(1):1–29

Wickham H (2016) Ggplot2: elegant graphics for data analysis. Springer-Verlag, New York, NY

Editorial responsibility: Toshi Nagata, Kashiwanoha, Japan
Reviewed by: 3 anonymous referees

Submitted: January 14, 2021
Accepted: August 27, 2021
Proofs received from author(s): November 7, 2021